JOM manuscript No.
(will be inserted by the editor)

Implications of the direct use of slag from ironmaking processes as a molten oxide electrolyte

Samuel Martin-Treceno · Antoine Allanore · Catherine M. Bishop · Aaron T. Marshall · Matthew J. Watson

Received: date / Accepted: date

Abstract The thermochemical and electrical behaviour of ironmaking slag produced from titanomagnetite concentrates was assessed in the vicinity of its tapping temperature. A combination of electrochemical measurements in a modified thermal imaging furnace and computational thermodynamic calculations was employed to elucidate its potential use as a molten oxide electrolyte for the extraction of high-purity metal. The results show that the presence of entrained iron species in the ironmaking slag decreases the faradaic efficiency of the electrolysis. Thermodynamic predictions reveal a small electrochemical window of operation between the decomposition of silica and titania, which might result in the co-reduction of titanium and silicon ions from the melt. Practical considerations for the electrochemical production of metal directly from the ironmaking process are discussed, and further experimental investigation of the electrochemical behaviour of this material is justified.

Corresponding author email: catherine.bishop@canterbury.ac.nz

S. Martin-Treceno, A. T. Marshall, M. J. Watson

Department of Chemical and Process Engineering, University of Canterbury, Christchurch, New Zealand

A. Allanore

Department of Materials Science and Engineering, Massachusetts Institute of Technology, Cambridge, MA 02139, USA

C. M. Bishop

Department of Mechanical Engineering, University of Canterbury, Christchurch, New Zealand

Keywords molten oxide electrolysis · electrolyte · characterization · titanium bearing slags · blast furnace slag

1 Introduction

With the increase in environmental awareness and the world's population predicted to reach 10 billion by 2050 [1], metal extraction industries are revisiting their technologies for alternative solutions to meet current and future demand for materials in a sustainable manner. The direct electrochemical decomposition of metal-bearing compounds has been demonstrated at the laboratory and pilot scales as an alternative carbon-free production route [2,3], capable of minimizing the total use of carbon or fuel compared to the current metal extraction processes. Aluminum's Hall-Heroult process illustrated the potential of electrochemical processing to mass-produce high purity metals [4]. The electrolysis of iron in a molten oxide electrolyte [5] and copper in a molten sulfide electrolyte [6] are promising solutions, where O_2(g) and S_2(g) are the only by-products; although, much work is needed to take these to industrial scale. While molten sulfides remain understudied [7], recent governmental efforts to reduce carbon dioxide emissions have brought research attention to molten oxide electrolysis (MOE) [8].

The use of ironmaking slag as a secondary source of metal has been postulated [9] as a promising alternative to address the universal need to recycle large-scale waste materials. In 2019, between 320 and 384 million tonnes of ironmaking slag were produced worldwide [10]. These slags can contain up to 30 wt.% TiO_2 [9] and are available at 1773 K as a by-product of the ironmaking process in countries such as China, South Africa and New Zealand. The use of this material as a molten oxide electrolyte has the potential to reduce emissions to the environment, stop land-fill disposal [11], and reduce energy inefficiency of the overall steelmaking process [12]. Furthermore, based on the relative content of each material[1], ironmaking slag is more than 10 times cheaper as a source of titanium than ilmenite, the most common feedstock for titanium production. Today, steelmakers typically contract outside processing companies to dispose of the slag. These companies tend to receive the slag for free, process it, and

[1] Calculations were made based on slags with 30 wt.% TiO_2 [9] and 54 wt.% TiO_2 for ilmenite [13]. Selling prices for air-cooled ironmaking slag average 8.53 USD per tonne [14] and 180 USD per tonne for ilmenite [13].

pay a small percentage of the sale revenue back to the steelmaker [14].

The extraction of titanium metal from slag has been studied in the past with limited success [15]. The scattered distribution of titanium in various mineral phases with complex interfacial combinations yields very low recovery rates with the use of traditional separation techniques in cooled slag [16]. The use of the slag directly from the process, in its molten state, to electrochemically extract high-purity metal is proposed in this work as a pathway towards clean metal production that enables tapping into all the available titanium and uses the embodied heat.

One of the major challenges towards this clean metal production route is the complexity of determining the properties of the electrolytes at the operating temperatures. The high temperatures required for operation and the highly corrosive nature of the oxide melts have traditionally imposed very demanding material constraints [17,18], hindering the required characterization at temperature. Schiefelbein and Sadoway [19] pointed to silicate melts as promising candidate electrolytes for MOE, but highlighted the general lack of data to assess the properties of the melts. Experimental data is scarce and only available for selected temperatures and composition ranges [20], so researchers mainly rely on empirical models [21] backed by computational thermodynamic calculations [22]. Nevertheless, motivated by recent technological advances [23], this work provides a comprehensive study of ironmaking slags produced from titanomagnetite concentrates with respect to their use as an electrolyte in prospective high-temperature electrochemical processes.

For the practical implementation of an electrochemical route to extract titanium, at the operating conditions the ironmaking slag should (a) have high solubility for TiO_2, (b) be molten, (c) have sufficient ionic conduction, and (d) present metal oxide constituents that are more thermodynamically stable than TiO_2. When considering the industrial application of such a route, there are, of course, additional properties that an ideal electrolyte should possess to optimize the process for commodity metal extraction. The electrolyte should be inexpensive and, ideally, benign to the environment. This material needs to be stable at the range of oxygen partial pressures experienced at the electrodes. Additionally, in order to efficiently harvest the metal produced, the electrolyte must be less dense than the product and have low

viscosity so it facilitates the movement and separation of charged species. Also, ideally, if a liquid metal pool is formed, the electrolyte should wet it.

In this work, a combination of electrochemical measurements in a modified thermal imaging furnace and computational thermodynamic calculations was used to characterize the potential use of ironmaking slag, directly from the ironmaking process, in an MOE cell. The aim of this paper is to assess the feasibility of extracting titanium metal from ironmaking slag. Consequently, the focus was on investigating the constraints arising from operating directly from the process, *i.e.*, presence of entrained iron in the slag; the electrical conduction of the slag, in particular, the fraction of the charge that goes to the reaction of interest; and the thermodynamic stability of the melt components, crucial for an efficient process and a pure metal product. This paper provides the knowledge required for an effective use of the ironmaking slag as electrolyte in an MOE process, and highlights the effect of iron, often overlooked in the literature where ironmaking slag is normally treated as $TiO_2 - SiO_2 - Al_2O_3 - MgO - CaO$.

2 Experimental

2.1 Sample - origin

In ferrous metallurgy, the raw materials determine the amount of titania present in the slag phase formed during the ironmaking process. In New Zealand and China, the fraction of titania in the slag comes from the use of titanomagnetite deposits, commonly referred to as ironsands, as the source of iron in the ironmaking process [9]. These mineral deposits are first concentrated by magnetic and gravity separation processes [24]. Davis Tube tests [25] indicated that the strongly magnetic constituents separated are rich in iron and correspond to 20 wt.% ± 5 wt.% of the total sand weight. This concentrate, commonly referred to as primary concentrate, is the feedstock of the ironmaking process alongside coal and fluxes. Depending on the type of process, the last steps of the reduction process and the phase separation occur in a blast furnace or in an electric furnace. In both cases, the pig iron is tapped from the bottom of the furnace. On top of the iron, an oxide layer is formed containing all the remaining elements. This less dense, left-over phase is what is commonly referred to as slag, and it contains a certain amount of dissolved and entrained iron (Table I). The compositions of titanomagnetite sand, primary concentrate and ironmaking slag samples used are representative of the local, New Zealand ironmaking process and

TABLE I. Titanomagnetite sand, primary concentrate and ironmaking slag compositions (wt.%) measured by XRF.

	TiO_2 wt.%	CaO wt.%	SiO_2 wt.%	Al_2O_3 wt.%	MgO wt.%	Fe_3O_4 wt.%	MnO wt.%	V_2O_5 wt.%
Titanomagnetite sand	1.8	12.6	46.2	9.0	8.6	12.9	0.4	0.1
Primary Concentrate	7.9	0.5	2.3	3.7	2.9	81.4	0.6	0.5
Slag#1	32.5	16.4	13.8	18.5	13.6	4.3	0.9	0.2

were measured by X-ray fluorescence spectroscopy (XRF, Bruker S8 TIGER running a 4kW Rhodium tube). The multivalent species, iron and titanium, are reported as wt.% Fe_3O_4 and TiO_2, respectively, as the samples were heated to 1273 K to obtain the most stable oxides before the XRF measurement.

The slag's stability over time is an important parameter that influences the quality of the final product (Figure 1). With an average of more than 30 wt.% of TiO_2 dissolved within, ironmaking slags from titanomagnetite concentrates present concentrations of the target metal cations higher than common industrial electrolytes such as cryolite [26]. From such a standpoint, the high solubility of the metal cations of interest in this molten oxide system makes it an ideal candidate for future industrial applications [7].

2.2 Analytical methods

A thermal imaging furnace (TX-12000-I-MIT-VPO-PC, Crystal Systems Corp.) that had been previously modified to carry out electrochemical measurements [23] was used to study the electronic conduction of the slag from 1773 to 1933 K, without container compatibility constraints. This containerless method uses the pendant droplet technique to configure the electrochemical cell, which has been described and elsewhere [27]. UHP Ar (99.999%, Airgas Inc.) was used inside the furnace during operation at a flow rate of 200 mL min^{-1} yielding a partial pressure of oxygen of 10^{-6} atm. The furnace lamp power-sample temperature relations were determined for the various samples by contacting the molten droplet with a type C (W-Re (5 wt.%) — W-Re (26 wt.%)) thermocouple (Figure 2).

Stepped-potential chronoamperometry was used to perform transference number measurements in the thermal imaging furnace. Fried *et al.* [28] proved this technique capable of differentiating between

the ionic and electronic conduction in titanate melts. Even though there is no standardised technique to measure transference numbers in corrosive, ultra-high melting temperature electrolytes such as the $TiO_2-SiO_2-Al_2O_3-MgO-CaO$ slag, Olsen *et al.* [29] proved that the stepped-potential chronoamperometry can be as effective as the predominant Hittorf method. Hence, in this paper, this technique is used to provide an estimate of the contribution of the ionic and electronic charge carriers to the total current (I_t). The electronic (t_e) and ionic (t_i) transference numbers obtained have been used before to quantify the current associated with the flow of electrons (I_e) and ions (I_i), respectively, in mixed conducting media [30,31,28,32,33,29], where both contributions sum to unity:

$$t_i + t_e = \frac{I_i}{I_t} + \frac{I_e}{I_t} = 1 \tag{1}$$

For each measurement, iridium wires (Ir > 99.9 %, diameter = 0.5 mm, Furuya Metals Co. Ltd.) were used in a three-electrode configuration inside an Al_2O_3 four-bore tube. Using a potentiostat (Gamry Reference 3000), the open circuit potential was recorded to confirm that the electrodes had contacted the molten slag droplet. For each transference number measurement, the working electrode was maintained at open circuit potential for 15 s before being stepped to 0.01 V vs Ir for 30 s. 100 measurements per second were recorded to accurately capture the potential step. The transference numbers can be calculated from the current response to the potential step as a function of time [30]. In particular, the electronic transference number is calculated by dividing the initial ($t \to 0$) from the long-time ($t \to \infty$) values of the current (I) using:

$$t_e = \frac{I_{t\to\infty}}{I_{t\to 0}} \tag{2}$$

Additionally, 10 g of Slag#1 were heated (GSL-1700x-100VT-UL tube furnace, MTI Corp.) in graphite crucibles (Baofeng Graphite) under a Ar (99.999 %, BOC) atmosphere to 1723 and 1823 K to simulate the conditions found in the industrial ironmaking process. The heating and cooling rate was 1 K min^{-1} and the samples were held at temperature for 360 min. For the post-experiment analysis, the samples were cross-sectioned upon cooling using a high-speed diamond saw (Bühler), set in a conducting mounting compound (ProbeMet), and polished using progressively finer grades of silicon carbide paper (180, 320, 400, and 600 grit) and a diamond suspension with an average particle size of 9 μm. The composition and microstructure of the sample were examined using a scanning electron microscope (SEM, JEOL JSM-IT300LV) with LaB6 filament equipped with a X-Maxä 50 silicon drift energy dispersive spectroscopy (EDS) detector with a working distance of 9.5 mm and accelerating voltage of 20.0 kV.

2.3 Thermodynamic predictions

Equilibrium reduction potentials for the electrolytic extraction of metals from slags were predicted with FactSage 7.2 [34]. The thermodynamic (minimum) cell voltage required for the reduction of metal ions from the slag with simultaneous O_2 evolution (E_{cell}) was calculated using the Nernst equation:

$$E_{cell} = -\frac{\Delta G^{\circ}}{nF} - \frac{RT}{nF} \cdot \ln \frac{\prod a_{products}^{\nu}}{\prod a_{reactants}^{\nu}} \tag{3}$$

where F is the Faraday constant and n is the number of electrons involved in the reaction. R, T and ν are the universal gas constant, the temperature of interest and the stoichiometric coefficients from the overall cell reaction, respectively. ΔG° is the standard Gibbs energy of the dissociation reaction at unit activity in pure component state, and a_i is the activity of the *ith* species in the reaction at cell conditions. Model parameters were obtained from FactSage's FToxid and FactPS databases [34], where the molten slag phase is described using an optimized Modified Quasichemical Model [35]. The thermodynamic activities for the components of the molten slag system were obtained from this validated solution model [22], while unit activity was chosen for the metal and oxygen gas. To simulate the conditions in the ironmaking process, the oxygen activity in the slag phase was determined by equilibrium with a gas whose oxygen activity was determined by equilibrium with graphite.

3 Results and Discussion

3.1 Chemical considerations

In MOE, the choice of supporting electrolyte is the single most important process parameter. For the current study, the composition of the electrolyte was fixed as the study focused on the direct use of ironmaking slag from the process, without the use of a supporting electrolyte. The elemental composition of Slag#1 given in Table I reports iron as Fe_3O_4 since the sample was oxidized before XRF measurements, but iron in melter slag at process conditions would be in the form of low valency iron ions, FeO, and metallic iron [36,37]. This is mostly due to the operating conditions of the melter, where a liquid pool of pig iron metal forms at the bottom as the carbon content in the pig iron (around 3.40 wt.% [38]) reduces the melting point of the metal product about 300 K. There, most iron will be metallic and in equilibrium with Fe^{2+} in the slag. Little Fe^{3+} is expected, as hematite decomposes spontaneously at those temperatures and oxygen partial pressures[5,37]. If equilibrium between slag and pig iron were

obtained, then metal entrainment is expected to account for the iron present in the electrolyte straight from the industrial source. Due to significant deviations from equilibrium in the electric arc furnace, the relative contributions from entrained and dissolved iron would need to be determined, for example, with wavelength dispersive spectroscopy [39].

A significant number of small metallic droplets were observed on the surface of Slag#1 after it was fired in a graphite crucible at 1723 K (Figure 3A). There were fewer metal droplets on top of the slag (Figure 3C) and most were suspended near the bottom of the crucible (Figure 3D) for Slag#1 cooled from 1823 K. The large bubbles suspended in the solidified slag in Figure 3B, and, to a lesser extent in Figure 3D, illustrate the viscous nature of the slag. An increase in temperature should decrease the viscosity, reducing the amount of entrained iron in the slag. While this may have allowed more droplets to sink under gravity, droplet coalescence was still hindered by metal carbide formation, the presence of which has been reported to cause a rapid increase in the viscosity of slags [40,41,36].

At the strongly reducing conditions of the melter, due to the large carbon electrodes, V_2O_5 and TiO_2 in the molten slag can react with carbon to form mixed metal carbide precipitates [42]. Metallic iron is trapped by those solid carbide particles in the slag. The carbides heterogeneously nucleate at the metal-slag interphase interface [36], which inhibits the growth and coalescence of metallic iron droplets [41]. The carbide shells of several smaller droplets that have coalesced before solidification are visible in the V and Ti X-ray maps in Figure 4.

Zhang *et al.* [41] found that TiC can be oxidised easily under dynamic oxidation conditions, causing a rapid decrease in the viscosity of the slag. Hence, increasing the oxygen chemical potential enables iron droplets to coalescence, facilitating the separation of iron from the slag [36]. This is consistent with the large metallic iron droplet found at the base of the quenched pendant droplet of molten slag formed during experimentation in the thermal imaging furnace at $P_{O_2} = 10^{-6}$ atm (Figure 5A). The containerless method meant there was no carbon available for carbothermal reduction. Thus, we conclude that the metal carbide precipitates had a larger effect on the viscosity than changing temperature.

3.2 Electrical considerations

In order to consider ironmaking slag a successful electrolyte, it is desirable that it possesses acceptable values of total electrical conductivity [19]. Following Ohm's law, a high total electrical conductivity is desired to maximize the production of the target metal as it will enable greater current densities for a given applied voltage. For comparison, the total electrical conductivity for pure cryolite is reported to be 2.8 S cm^{-1} [43] at 1273 K. For Ti-bearing blast furnace slag with 23 wt.% TiO_2 and 4.8 wt.% FeO, Wang *et al.* [44] reported a conductivity of 1.2 S cm^{-1} at 1773 K. At that temperature, increasing TiO_2 to $>$ 70 wt.% increased the total electrical conductivity up to 100 S cm^{-1} [45]. This range suggests that the total electrical conductivity of titanium-bearing slags can be tuned to the requirements for a successful industrial electrolyte.

Oxide melts are mixed conductors [30,46] so, to maximize metal production, the fraction of charge carried by electrons is also important. On one side, electronic conduction wastes energy as the movement of electrons is not linked to the production of metal and lowers the faradaic efficiency [47]. However, some electronic conduction is beneficial for Joule heating to satisfy the thermal needs of the process [48]. Hence, to produce metal at an economically viable rate, the total electrical conductivity should be maximized and the electronic conduction minimized [49]. We postulated that, due to the mixed oxide nature of the slag, the fraction of the charge carried by ions will be high enough to sustain a current efficiency that enables high production rates while minimizing energy consumption. Using the slag directly from the melter (T $>$ 1773 K) should promote ionic mobility, and may enable a solvent-free process, *i.e.*, no additional electrolyte component would be needed.

The ionic conduction was investigated as a function of temperature in the vicinity of the tapping temperature (Figure 6). The effect of changing temperature was minor, and the ionic transference numbers were $t_i \approx 0.53 - 0.61$ for Slag#1. The ionic conduction in the slag depends on the concentration, charge, and mobility of charge carriers [50]. As all the measurements were done at the same partial pressure of oxygen, the variation of the degree of polymerization of the melt as a function of temperature is expected to be the main factor influencing ionic conduction. For ironmaking slags, Liao *et al.* [51] illustrated that the viscosity does not change much above 1773 K, with values less than 0.5 Pa s reported [20]. The negligi-

ble effect of temperature on the ionic conduction above 1773 K can be associated with the viscosity of the slag being stable at the operating temperatures and too low for mass transport to limit current efficiency.

The effect on the transference numbers of the iron content in the ironmaking slag was also investigated. The total concentration of Fe in a sample was reduced by separating the metallic droplet from the bottom of a quenched pendant droplet of Slag#1 (Figure 5A). The concentration of Fe was not measured post operation, but Zhang *et al.* [41] reported a decrease from 2.50 wt.% to 0.07 wt.% after the metallic Fe in a Ti-bearing blast furnace slag had coalesced. In this work, the ionic transference numbers for Slag#1 with Fe droplet removed (squares in Figure 6) were higher than for Slag#1.

If the liquid metal and slag phases are at equilibrium at some temperature, then the composition of the slag phase will not change by removing any of the metallic phase at that temperature. The transference numbers of Slag#1 (circles) and Slag#1 with metal droplet removed (squares) differ when measured under the same experimental conditions (Figure 6.) This suggests that even though the pendant droplet samples were quenched, the metallic droplet and slag phase when they were separated were not in thermodynamic equilibrium representative of the measurement temperatures for chronoamperometry. One explanation could be that metallic droplet of various sizes could be entrained in the slag phase. The amount of Fe in the slag in equilibrium with the smallest metallic droplets will be higher than the amount in equilibrium with the largest droplet due to the Gibbs-Thomson effect. When the large droplet is removed and the system remelted, the remaining very small metallic droplets can coalesce with time at temperature, and the amount of Fe in equilibrium with the now remaining larger metal droplet will shift to lower Fe concentrations. Due to the small sizes, this droplet size solubility limit effect can be significant.

Rouaut *et al.* [49] compared the electronic conductivity of cryolitic melts with and without metals, and highlighted the dissolved aluminum metal as a source of mobile electrons. In metal-molten salt systems, dissolved metal not only increases the total electrical conductivity of the molten electrolyte by providing highly mobile electrons, but it decreases the faradaic efficiency of the electrolysis as the dissolved aluminum is reoxidized by the gas evolved at the counter electrode. Furthermore, the presence

of multivalent iron is known to increase the electronic conductivity of the slag [32].

The gain of efficiency by removing multivalent iron from the melt was confirmed by performing transference number measurements on an iron-free TiO_2 - SiO_2 - Al_2O_3 - MgO - CaO slag sample prepared from high purity precursors (see [27] for details). This showed that the ionic transport was indeed higher with the iron-free slag (diamonds in Figure 6).

To put these results into perspective, cryolite as a supporting electrolyte yields $t_i \approx 1$ at industrial operating conditions [52]. *A priori*, this suggests that an electrochemical route using ironmaking slag directly might be far from the creation of a commodity-cost extraction process analogous to aluminum's Hall-Heroult process; however, the elevated cost associated with upstream processing to convert bauxite ore to Al_2O_3 and the low concentration of Al_2O_3 in cryolite ($2-5$ wt.% [53]) are constraints that could be avoided with our proposed route. It is worth noting that newly established routes, such as the FFC process, report similar characteristics *i.e.* a faradaic efficiency of 50% and a solid product [54]. It is out of the scope of this work to discuss the optimal operational parameters for the electrolysis of molten ironmaking slag, but to encourage further exploration of its electrochemical behaviour.

3.3 Thermodynamic considerations

The stability of the metal oxide constituents at the operating conditions must be investigated as their decomposition will limit the operating temperature of the MOE cell [26] and the purity of the final metallic product.

3.3.1 Thermal stability

The Gibbs energy for the dissociation reactions of the pure compounds in their standard state, $\Delta G^{\circ}_{decomp}$, is given in Table II. At 1773 K, the thermal stability of all the pure major components found in the slag ($\Delta G^{\circ}_{decomp} > 0$) is guaranteed. No constituent of the electrolyte will decompose spontaneously into pure metal and oxygen gas.

TABLE II. $\Delta G^{\circ}_{decomp}$, E°_{cell} and E_{cell} for the decomposition reactions in the proposed electrolyte, Slag#1, at 1773 K predicted with FactSage.

	$\Delta G^{\circ}_{decomp}$ / **kJ mol^{-1}**	E°_{cell} / **V**	E_{cell} / **V**
$CaO\ (s) \rightleftharpoons Ca\ (l) + \frac{1}{2}\,O_2\ (g)$	445	-2.30	-2.68
$MgO\ (s) \rightleftharpoons Mg\ (g) + \frac{1}{2}\,O_2\ (g)$	367	-1.90	-2.06
$Ti_2O_3\ (s) \rightleftharpoons 2\,Ti\ (s) + \frac{3}{2}\,O_2\ (g)$	1044	-1.80	-2.02
$Al_2O_3\ (s) \rightleftharpoons 2\,Al\ (l) + \frac{3}{2}\,O_2\ (g)$	1108	-1.91	-2.01
$TiO_2\ (s) \rightleftharpoons Ti\ (s) + O_2\ (g)$	627	-1.62	-1.88
$SiO_2\ (s) \rightleftharpoons Si\ (l) + O_2\ (g)$	596	-1.54	-1.75
$MnO\ (s) \rightleftharpoons Mn\ (l) + \frac{1}{2}\,O_2\ (g)$	251	-1.30	-1.68
$FeO\ (l) \rightleftharpoons Fe\ (s) + \frac{1}{2}\,O_2\ (g)$	153	-0.79	-1.44
$Fe_3O_4\ (s) \rightleftharpoons 3\,Fe\ (s) + 2\,O_2\ (g)$	560	-0.73	-1.33
$V_2O_5\ (l) \rightleftharpoons 2\,V\ (s) + \frac{5}{2}\,O_2\ (g)$	876	-0.91	-1.32

3.3.2 Electrochemical stability

In non-aqueous electrochemistry, the selectivity of the process requires the exclusive reduction of the metal ions of interest from the melt [55]. Hence, to produce a high-purity metal and O_2(g) from the electrolysis of molten slag, the melt must be free of elements more noble than the metal of interest [19]. The thermodynamic (minimum) cell voltage at standard conditions (E°_{cell}) was calculated from $\Delta G^{\circ}_{decomp}$ and indicates that the relative stability of the metals as oxides at 1773 K is Fe < V < Mn < Si < Ti < Mg < Al < Ca. However, molten oxides are complex, non-ideal solutions [22], and the relative stability of the components in the melt assessed by E°_{cell} fails to take into account the electrolyte composition or thermodynamic activities. Using the Nernst equation, the minimum potential difference between the working and counter electrodes required for a redox reaction to occur (E_{cell}) was calculated at 1773 K, Table II. The relative stability of the metals as oxides at 1773 K changes to V < Fe < Mn < Si < Ti < Al < Mg < Ca.

The calculated E_{cell} are consistent with the electrochemical reduction of titanomagnetite ironsand reported by Bjareborn *et al.* [56]. The formation of V, Fe and Mn should occur first. Hence, a multistage electrolysis could be performed to extract these minor components of the slag first. The small potential window between the reduction of Si and Ti indicates that they might co-reduce from the melt and form

Ti_xSi_y intermetallic phases (Table II). But it may also imply that the deposition series could be altered by modifying the composition of the electrolyte or the concentration of the electronegative species (*e.g.*, through the use of a supporting electrolyte [57,55]), which was out of scope of this study. Regardless, producing titanium silicides is a promising high added-value alternative [58]. Either way, the results presented in this paper justify further study of the electrochemical behaviour of this oxide system to investigate the kinetics of the reduction process and determine its potential as a secondary source of metals.

4 Conclusions

The implications of using TiO_2-rich ironmaking slag as a molten oxide electrolyte were investigated. To assess the feasibility of producing high-purity metal directly from the ironmaking process, the following considerations must be taken into account:

- Operating in the vicinity of the tapping temperature of the slag did not have a significant effect on the charge transfer in the molten oxide.
- Iron in the melt, even in small quantities, considerably increased the electronic conduction in the melt, hindering the faradaic efficiency of the process.
- If pure Ti metal is the desired product, the melt should be free of all Fe, V and Mn because it is easier to reduce than the target metal.
- The proximity of the thermodynamic cell voltages for the reduction of Si and Ti ions from the melt calls for an electrochemical study to understand the overpotentials at the electrodes, which will ultimately control the composition of the metal produced.

The results presented in this paper, alongside the timely need to recycle large-scale waste materials, motivate further exploration of the electrochemical behaviour of titanium-bearing slags relevant for MOE.

Conflict of interest

On behalf of all authors, the corresponding author states that there is no conflict of interest.

Acknowledgements The authors thank BlueScope Steel for samples. This research was funded by the New Zealand Ministry of Business, Innovation and Employment (MBIE) under contract CONT-46287-CRFSI-UOC.

References

1. UN Department of Economic and Social Affairs, Population Division, World population prospects: The 2017 revision:Key Findings and Advance Tables. Working paper no. ESA/P/WP/248. Tech. rep., United Nations New York, NY (2017)
2. G.Z. Chen, D.J. Fray, T.W. Farthing, Nature **407**(6802), 361 (2000)
3. A. Allanore, L. Yin, D.R. Sadoway, Nature **497**(7449), 353 (2013). DOI 10.1038/nature12134
4. A. Allanore, Electrochimica Acta **110**, 587 (2013). DOI http://dx.doi.org/10.1016/j.electacta.2013.04.095
5. J. Wiencke, H. Lavelaine, P.J. Panteix, C. Petitjean, C. Rapin, Journal of Applied Electrochemistry **48**(1), 115 (2018). DOI 10.1007/s10800-017-1143-5
6. K. Daehn, A. Allanore, Current Opinion in Electrochemistry (2020). DOI 10.1016/j.coelec.2020.04.011
7. A. Allanore, The Electrochemical Society Interface **26**(2), 63 (2017)
8. C. Bataille, M. Ahman, K. Neuhoff, L.J. Nilsson, M. Fischedick, S. Lechtenbohmer, B. Solano-Rodriquez, A. Denis-Ryan, S. Stiebert, H. Waisman, O. Sartor, S. Rahbar, Journal of Cleaner Production **187**, 960 (2018). DOI 10.1016/j.jclepro.2018.03.107
9. S. Martin-Treceno, C. Bishop, A. Marshall, M. Watson, in *Chemeca 2018* (Institution of Chemical Engineers, Queenstown, NZ, 2018), pp. 28.1–28.9
10. K.C. Curry. U.S. Geological Survey, Mineral Commodity Summaries: Iron and Steel Slag. https://pubs.usgs.gov/periodicals/mcs2020/mcs2020-iron-steel-slag.pdf (accessed: 2020-09-30)
11. R. Dippenaar, Ironmaking & Steelmaking **32**(1), 35 (2005). DOI 10.1179/174328105X15805
12. B. Lin, H. Wang, X. Zhu, Q. Liao, B. Ding, Applied Thermal Engineering **96**, 432 (2016). DOI 10.1016/j.applthermaleng.2015.11.075
13. J. Gambogi. U.S. Geological Survey, Mineral Commodity Summaries: Titanium Mineral Concentrates. https://pubs.usgs.gov/periodicals/mcs2020/mcs2020-titanium-minerals.pdf (accessed: 2020-09-30)
14. H.G. Van Oss, Slag-iron and steel [Advance release]. 2016 minerals yearbook, U.S. Geological Survey (2018)
15. L.S. Li, Z.T. Sui, Acta Physical Chemistry Sinica **17**, 845 (2001)
16. X.F. She, H.Y. Sun, X.J. Dong, Q.G. Xue, J.S. Wang, Journal of Mining and Metallurgy, Section B: Metallurgy **49**(3), 263 (2013)
17. E. Standish, D. Stefanescu, P. Curreri, in *47th AIAA Aerospace Sciences Meeting Including the New Horizons Forum and Aerospace Exposition* (2009). DOI 10.2514/6.2009-1657
18. A.Y. Ilyushechkin, M.A. Duchesne, S.S. Hla, A. Macchi, E.J. Anthony, Journal of Materials Science **48**(3), 1053 (2013). DOI 10.1007/s10853-012-6838-8
19. S.L. Schiefelbein, D.R. Sadoway, Metallurgical and Materials Transactions B **28**(6), 1141 (1997)
20. M. Allibert, *Slag Atlas*, 2nd edn. (Verlag Stahleisen, Düsseldorf, 1995)
21. K. Mills, L. Yuan, R. Jones, Journal of the Southern African Institute of Mining and Metallurgy **111**(10), 649 (2011)
22. I.H. Jung, M.A. Van Ende, Metallurgical and Materials Transactions B **51**(5), 1851 (2020). DOI 10.1007/s11663-020-01908-7
23. B.R. Nakanishi, A. Allanore, Journal of The Electrochemical Society **164**(13), E460 (2017). DOI 10.1149/2.1091713jes

24. N.Z. Steel. The history of ironsand. https://www.nzsteel.co.nz/new-zealand-steel/the-story-of-steel/the-history-of-ironsand/ (accessed: 2020-09-07)
25. V. Murariu, J. Svoboda, Physical Separation in Science and Engineering **12**(1), 1 (2003)
26. A. Allanore, Journal of The Electrochemical Society **162**(1), E13 (2015). DOI 10.1149/2.0451501jes
27. S. Martin-Treceno, N. Weaver, A. Allanore, C.M. Bishop, A.T. Marshall, M.J. Watson, Electrochimica Acta **354**, 136619 (2020). DOI 10.1016/j.electacta.2020.136619
28. N.A. Fried, K.G. Rhoads, D.R. Sadoway, Electrochimica Acta **46**(22), 3351 (2001). DOI 10.1016/S0013-4686(01)00531-X
29. I. Olsen, R. Koksbang, E. Skou, Electrochimica Acta **40**(11), 1701 (1995). DOI 10.1016/0013-4686(95)00094-U
30. M. Barati, K.S. Coley, Metallurgical and Materials Transactions B **37**(1), 41 (2006). DOI 10.1007/s11663-006-0084-x
31. S. Sokhanvaran, S. Thomas, M. Barati, Electrochimica Acta **66**, 239 (2012). DOI 10.1016/j.electacta.2012.01.077
32. A. Ducret, D. Khetpal, D.R. Sadoway, ECS Proceedings Volumes **19**, 347 (2002). DOI 10.1149/200219.0347PV
33. S.K. Ratkje, H. Rajabu, T. Førland, Electrochimica Acta **38**(2), 415 (1993). DOI 10.1016/0013-4686(93)85159-V
34. C. Bale, E. Belisle, P. Chartrand, S. Decterov, G. Eriksson, A. Gheribi, K. Hack, I.H. Jung, Y.B. Kang, J. Melancon, A. Pelton, S. Petersen, C. Robelin, J. Sangster, P. Spencer, M.A.V. Ende, Calphad-computer Coupling of Phase Diagrams and Thermochemistry **54**, 35 (2016). DOI 10.1016/j.calphad.2016.05.002
35. A.D. Pelton, M. Blander, Metallurgical Transactions B **17**(4), 805 (1986). DOI 10.1007/BF02657144
36. L. Zhang, W. Zhang, J. Zhang, G. Li, Metals **6**(5), 105 (2016). DOI 10.3390/met6050105
37. B. Sundman, Journal of phase equilibria **12**(2), 127 (1991)
38. N.Z. Steel. The ironmaking process. https://www.nzsteel.co.nz/new-zealand-steel/the-story-of-steel/the-science-of-steel/the-ironmaking-process/ (accessed: 2020-10-07)
39. I. Bellemans, E. De Wilde, N. Moelans, K. Verbeken, Advances in Colloid and Interface Science **255**, 47 (2018). DOI 10.1016/j.cis.2017.08.001
40. H. Du, Science Press, Beijing (1996)
41. L. Zhang, L. Zhang, M. Wang, G. Li, Z. Sui, ISIJ international **46**(3), 458 (2006)
42. Y. Chung, A.W. Cramb, Metallurgical and Materials Transactions B **31**(5), 957 (2000). DOI 10.1007/s11663-000-0072-5
43. J. Híveš, J. Thonstad, A. Sterten, P. Fellner, Metallurgical and Materials Transactions B **27**(2), 255 (1996). DOI 10.1007/BF02915051
44. S. Wang, G. Li, T. Lou, Z. Sui, ISIJ International **39**(11), 1116 (1999). DOI 10.2355/isijinternational.39.1116
45. K. Hu, X. Lv, W. Yu, Z. Yan, W. Lv, S. Li, Metallurgical and Materials Transactions B **50**, 2982 (2019). DOI 10.1007/s11663-019-01702-0
46. K.C. Mills, B.J. Keene, International Materials Reviews **32**(1), 1 (1987). DOI 10.1179/095066087790150296
47. J. Wiencke, H. Lavelaine, P.J. Panteix, C. Petitjean, C. Rapin, Journal of the Electrochemical Society **166**(14), E489 (2019). DOI 10.1149/2.0811914jes
48. S. Poizeau, D.R. Sadoway, in *Light Metals 2011 - TMS 2011 Annual Meeting and Exhibition, February 27, 2011 - March 3, 2011* (Minerals, Metals and Materials Society, 2011), TMS Light Metals, pp. 387–392
49. G. Rouaut, A.E. Gheribi, P. Chartrand, Journal of Fluorine Chemistry p. 109597 (2020). DOI 10.1016/j.jfluchem.2020.109597

50. S. Creager, in *Handbook of Electrochemistry*, ed. by C.G. Zoski (Elsevier, Amsterdam, 2007), pp. 57–72. DOI 10.1016/B978-044451958-0.50004-5

51. J.L. Liao, J. Li, X.D. Wang, Z.T. Zhang, Ironmaking and Steelmaking **39**(2), 133 (2012). DOI 10.1179/1743281211Y.0000000064

52. J. Híveš, P. Fellner, J. Thonstad, in *Molten Salts Chemistry and Technology* (John Wiley & Sons, Ltd, 2014), chap. 1.10, pp. 95–101

53. G. Haarberg, A. Sterten, H. Gudbrandsen, F. Olufsen, S. Rolseth, Light Metals-Warrendale pp. 367–370 (1998)

54. K. Mohandas, D. Fray, Trans. Indian Inst. Met **57**(6), 579 (2004)

55. M. Gibilaro, J. Pivato, L. Cassayre, L. Massot, P. Chamelot, P. Taxil, Electrochimica Acta **56**(15), 5410 (2011). DOI 10.1016/j.electacta.2011.02.109

56. O. Bjareborn, T. Arif, B. Monaghan, C.W. Bumby, Materials Research Express **7**(10), 106508 (2020). DOI 10.1088/2053-1591/abbd24

57. A. Abbasalizadeh, A. Malfliet, S. Seetharaman, J. Sietsma, Y. Yang, Journal of Sustainable Metallurgy **3**(3), 627 (2017). DOI 10.1007/s40831-017-0120-x

58. Z. Chen, Y. You, K. Morita, ACS Sustainable Chemistry & Engineering **6**(5), 7078 (2018). DOI 10.1021/acssuschemeng.8b00919

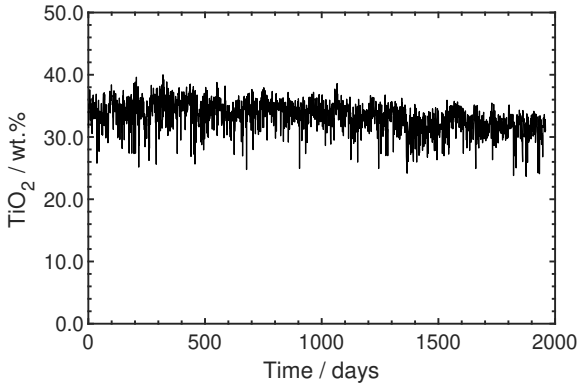

Fig. 1. Daily measurements of the TiO_2 concentration for tapped ironmaking slag representative of the local process in New Zealand over a period of four years, 2013-2017. Data supplied by BlueScope Steel.

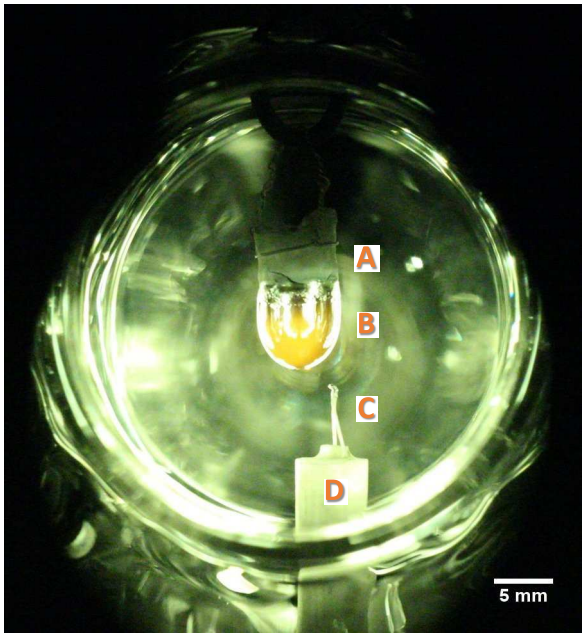

Fig. 2. Optical image of the pendant droplet captured through a flat window in the quartz tube by a camera (EOS Rebel T5i DSLR, Canon Inc.) with telescopic lens before it was contacted by a type C thermocouple, determining the operating temperature with ± 1% maximum error. (A) solid sintered sample suspended from the upper furnace by a Ni wire, (B) molten droplet formed as sample entered the hot zone, (C) exposed thermocouple wires, (D) four-bore alumina tube.

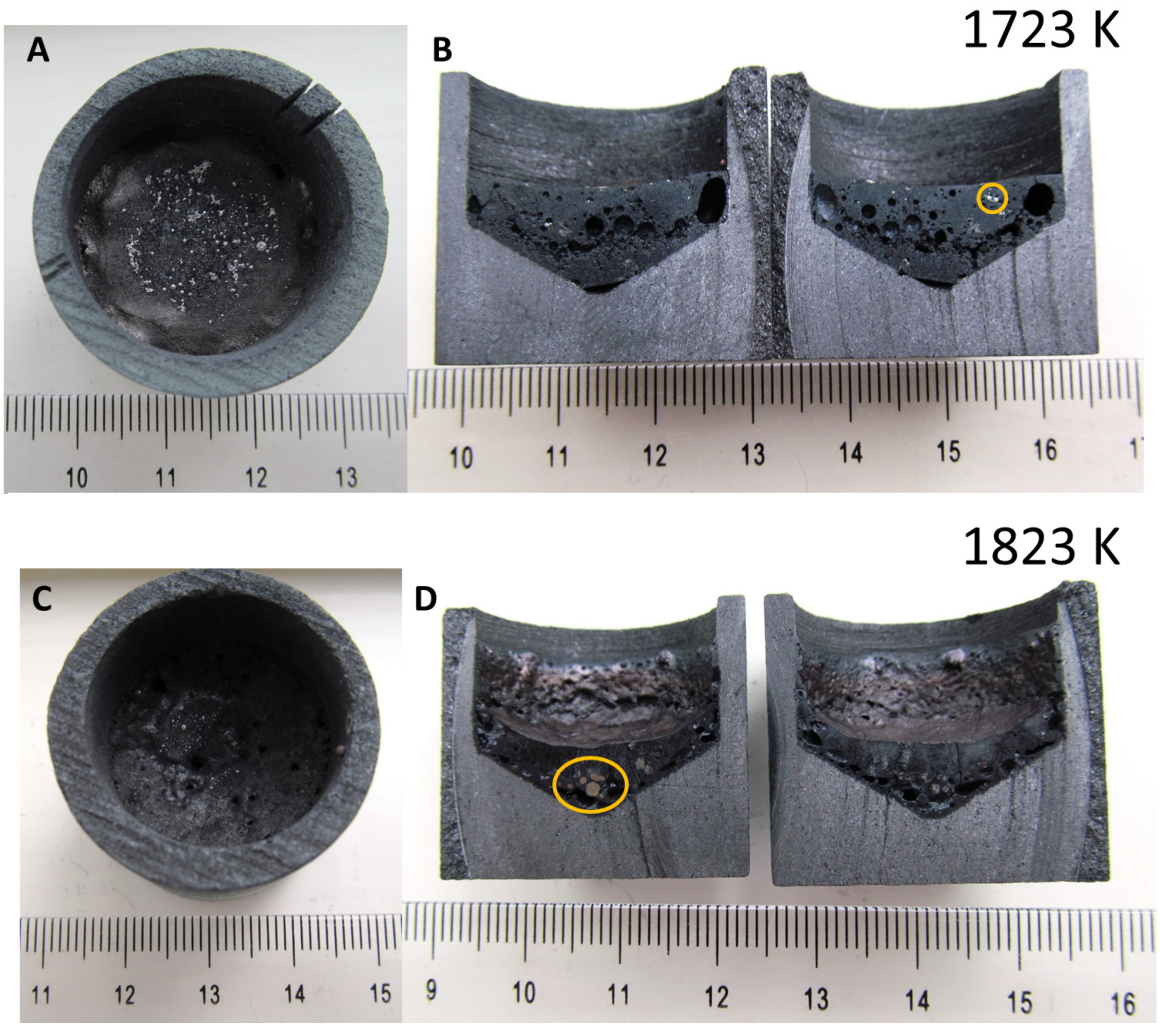

Fig. 3. Slag#1 after being fired in a graphite crucible under an argon atmosphere. (A) and (C) are plan views of the crucible showing a number of small metal beads on top of the slag. (B) and (D) are complete cross-section of the crucible showing entrained gas bubbles and metallic droplets. The yellow circle in (B) indicates the region analysed in Figure 4, where the yellow ellipse in (D) shows a region of metal droplets near the bottom of the crucible.

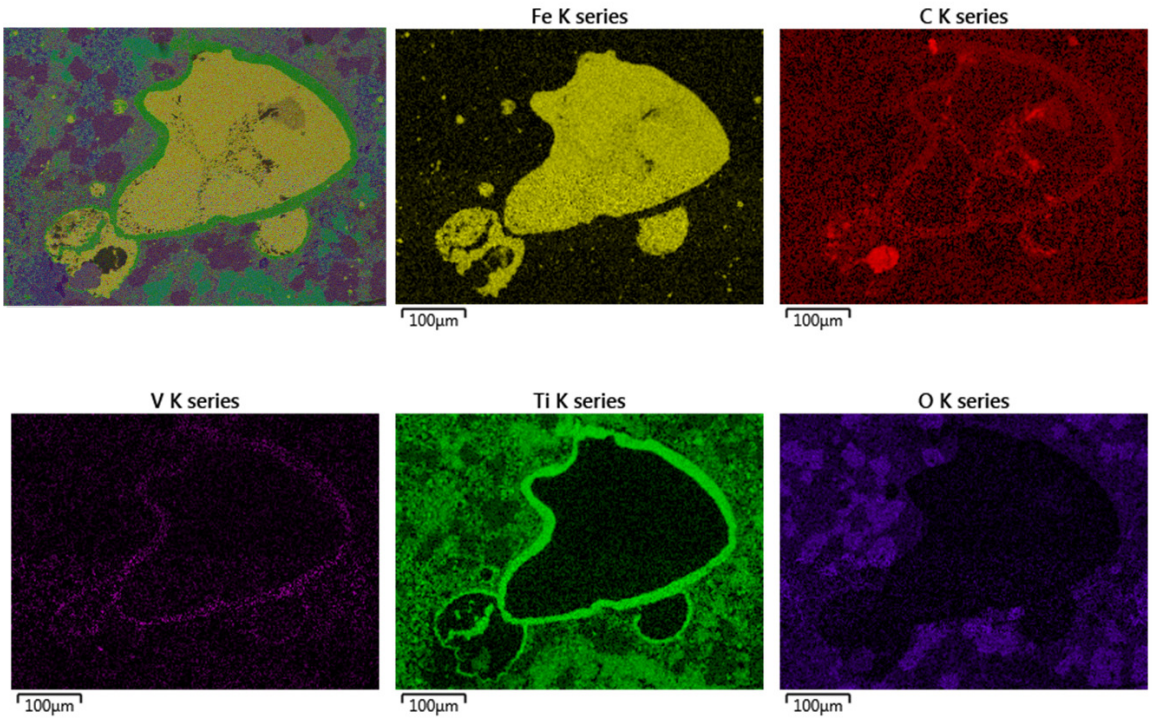

Fig. 4. EDS elemental composition maps illustrating the distribution of the major elements around a metallic iron drop suspended in Slag#1 at the region indicated in Figure 3 after cooling 1 K min^{-1} from 1723 K.

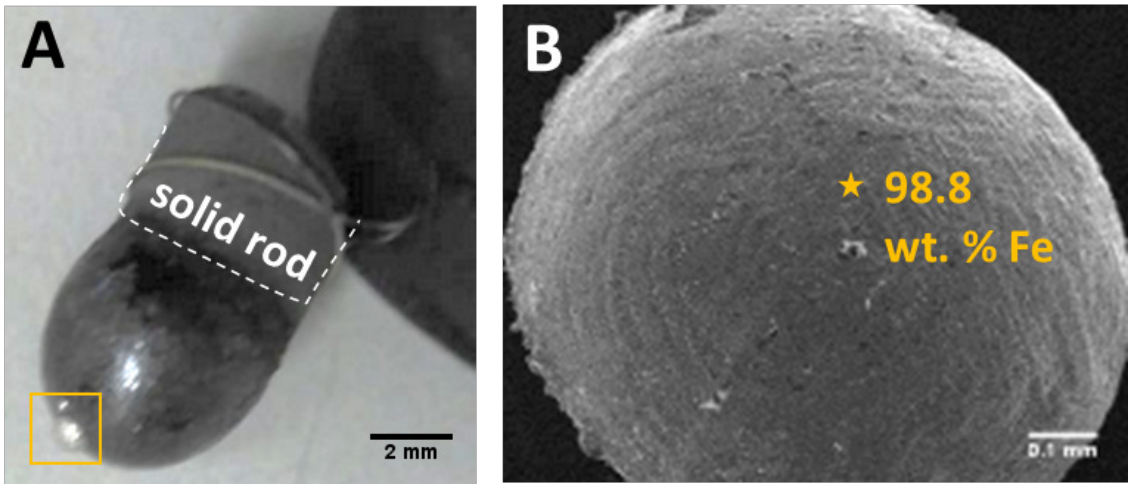

Fig. 5. Assessment of the metallic iron content in Slag#1. (A) Pendant droplet sample of Slag#1 after being quenched from 1823 K in the thermal image furnace at $P_{O_2} = 10^{-6}$ atm. The yellow square shows a metallic droplet that coalesced after melting and settled in the bottom of the pendant droplet. (B) Back-scattered image of the metallic droplet. The yellow star indicates the location of the compositional analysis reported on the image.

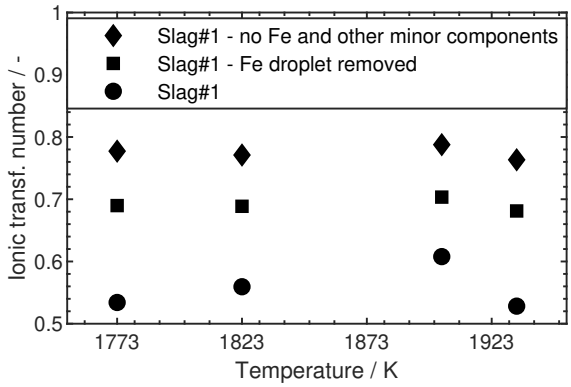

Fig. 6. Ionic transference number variation as a function of temperature for Slag#1 with different amounts of iron in its base composition for a partial pressure of oxygen of 10^{-6} atm. Values correspond to the average of two measurements, where the maximum average deviation measured was $\pm$ 0.014.